Ocean and Coastal Management 173 (2019) 52–64

Contents lists available at ScienceDirect

Ocean and Coastal Management

journal homepage: www.elsevier.com/locate/ocecoaman

Quantifying the impacts of human interventions on relative mean sea level change in the Pearl River Delta, China

Huayang Cai[a,b,c,d], Hao Yang[a,b,c,d], Junyong Liu[e], Lixia Niu[a,b,c,d], Lei Ren[a,b,c,d], Feng Liu[a,b,c], , Suying Ou[a,b,c,d,*], Qingshu Yang[a,b,c,d]

[a] Institute of Estuarine and Coastal Research, School of Marine Engineering and Technology, Sun Yat-sen University, Guangzhou, 510275, China
[b] State and Local Joint Engineering Laboratory of Estuarine Hydraulic Technology, Guangzhou, 510275, China
[c] Guangdong Provincial Engineering Research Center of Coasts, Islands and Reefs, Guangzhou, 510275, China
[d] Southern Laboratory of Ocean Science and Engineering (Guangdong, Zhuhai), Zhuhai, 519082, China
[e] The Pearl River Hydraulic Research Institute (PRHRI), Guangzhou, 510610, China

ARTICLE INFO

Keywords:
Relative mean sea level
Bivariate linear regression model
Human interventions
Climate change
Pearl River Delta

ABSTRACT

Due to the impact of both natural and human-induced changes, the hydrological regimes of many river deltas worldwide have been experienced either gradual or abrupt shifts. However, little work has explored the relative impacts of natural and human-induced changes on the natural balance of these delta systems. This study explores the overall influences of intensive human interventions (e.g., dam constructions, sand excavations, and land reclamations) on the relative mean sea level (RMSL) changes in the Pearl River Delta (PRD) in China. The analysis uses long-term measurements based on monthly averaged RMSL in 26 stations and reproduces the RMSL that would have occurred in the absence of large-scale human interventions by means of a simple bivariate linear regression model. Generally, we observe that the RMSL dynamics can be categorized into three distinct types, descending, ascending and fluctuant, according to the Mann-Kendall trend test. The analysis shows that the RMSL in the upper and central parts of the PRD displays a significant descending tendency owing to the deepening of the channels, which is primarily attributed to large-scale sand excavation. In contrast, for stations near the outlets, we observed an ascending tendency in RMSL that can be attributed to the combined effects of both the rise in global sea level and channel extension due to large-scale land reclamations. The regression model confirms that the human interventions have greater impacts in the upper and central parts of the PRD that feature river-dominated dynamics, compared with the lower parts of the PRD that are characterized by tide-dominated dynamics. In addition, the simulated results display a marked seasonal alteration in the RMSL: the alteration induced by human interventions is apparently greater during the flood season than it is during the dry season. The proposed method used here to quantify the impacts of both natural and human-induced interventions on the RMSL is particularly useful for setting scientific guidelines for water managements (e.g., flood control and salt intrusion prevention) and regulation projects (e.g., dam constructions and land reclamations) in river deltas.

1. Introduction

Change in the relative mean sea level (RMSL, defined as the sea level relative to the level of the local sea area), as a critical indicator of global climate change, exerts significant impacts on river delta systems, where the most densely populated areas are situated. Increasing evidence from both historical tide gauging observations and satellite altimetry indicates that the RMSL increased during the past two centuries due primarily to global warming and ice melting (Miller and Douglas, 2004; Church and White, 2006, 2011; Rignot et al., 2011). It was shown by the Intergovernmental Panel on Climate Change Fifth Assessment Report that the global mean sea level is projected to increase by 0.63–0.98 m by the end of the 21st century (Church et al., 2013; IPCC, 2014). However, owing to the influence of local factors (e.g., land subsidence or uplift and human interventions) the RMSL may vary greatly in both rate and magnitude. In particular, the cumulative impacts of human interventions and global climate change may lead to the exceeding of thresholds, beyond which the RMSL irreversibly changes,

* Corresponding author. Institute of Estuarine and Coastal Research, School of Marine Engineering and Technology, Sun Yat-sen University, Guangzhou, 510275, China.
E-mail address: ousuying@mail.sysu.edu.cn (S. Ou).

https://doi.org/10.1016/j.ocecoaman.2019.02.007
Received 25 July 2018; Received in revised form 8 January 2019; Accepted 16 February 2019
Available online 28 February 2019
0964-5691/

showing a notably decreasing trend. As concerns grow about the impacts of human interventions on the sustainable development of river delta systems (e.g., coastal flooding control, salt intrusion, shoreline erosion, and sustainable use of water resources), the need to understand changes in the RMSL in the context of global warming and intensive human interventions is receiving increasing attention (Schuttelaars et al., 2013; Wang et al., 2015; Zhou et al., 2017, 2018; Du et al., 2018; Wu et al., 2018).

Numerous studies have reported the RMSL rise and its impacts on river deltas all over the world (e.g., Ericson et al., 2006; Syvitski et al., 2009; Nicholls and Cazenave, 2010; Hinkel et al., 2014; Day et al., 2016; Tessler et al., 2018). Owing to the consistent RMSL rise, most river deltas worldwide are subject to increasingly vulnerable to submergence (conversion of coastal land to open ocean), flooding, as well as salt intrusion in estuaries (Nicholls and Cazenave, 2010). In particular, the vulnerability associated to RMSL rise is a result of the compound effects of climate-induced sea level rise (natural subsidence and global sea level rise) and human-induced changes (such as accelerated land subsidence due to groundwater and hydrocarbon extraction, reduced sediment supplies due to dam construction, floodplain engineering, and wetlands destruction). Much attention has been paid to the human-induced RMSL rise since most river deltas worldwide are sinking at rates much faster than global sea level is rising (Blum and Roberts, 2009; Syvitski et al., 2009; Wolinsky et al., 2010). This is particularly the true for the cases of deltas with virtually no aggradation and/or very high accelerated subsidence, such as Chao Phraya in Thailand, Colorado in Mexico, Krishna in India, Nile in Egypt, Po in Italy, Rhone in France, Sao Francisco in Brazil, Tone in Japan, and Pearl, Yangtze, Yellow in China (Syvitski et al., 2009). It should be noted that the estimated RMSL rise can be sensitive to spatial-temporal variability within individual deltas owing to the local human interventions (Tessler et al., 2018). Hence, to correctly assess the impacts of RMSL rise on delta systems and develop the long-term delta adaption strategies, it is required to quantify the spatial-temporal variations of RMSL over the whole river delta.

It is well known that changes in the dynamics of RMSL of river deltas are influenced by nonlinear interactions of riverine processes (represented by river discharge) with marine processes (represented by tidal waves). To be more specific, as river discharge debouches into the ocean, the RMSL is subjected to nonlinear tide-river interaction, which generates a steady gradient in the water surface that features various spatial (longitudinal and transverse) and temporal (spring-neap, wet-dry, interannual) scales (e.g., Godin and Martinez, 1994; Buschman et al., 2009; Sassi and Hoitink, 2013; Cai et al., 2014a,b, 2016; Hoitink and Jay, 2016; Hoitink et al., 2017). Recent studies showed that global climate change may influence the interannual variation of the RMSL through the alteration of river-tide dynamics by various processes, such as El Niño-Southern Oscillation (ENSO), Pacific Decadal Oscillation and La Nia events (e.g., Llovel et al., 2011; Cazenave et al., 2012, 2014; Wang et al., 2018a). On the other hand, human activities in the delta regions, including large-scale dam constructions, substantial land reclamations, sand excavations, dredging and various engineering works for flood protection, may significantly change the flow and tide regimes, thus altering the short-term (decadal variability) evolution of RMSL change.

The Pearl River Delta (PRD), located in the southern part of China, is the low-lying area surrounding the Pearl River channel networks (also known as Pearl River estuary), where the Pearl River flows into the South China Sea. It is one of the most densely urbanized and populated regions in the world and is subjected to strong human interventions. Many studies have been conducted to understand the impacts of human interventions on the hydrological and morphological regimes in the PRD (e.g., Zhang et al., 2009, 2010; 2015b, 2017, 2018; Wu et al., 2014, 2016a; 2016b, 2018; Liu et al., 2014, 2018a; 2018b; Cai et al., 2018). However, human interventions and global climate change take place concurrently. Therefore, the response of river delta systems to overall human interventions is difficult to quantify. To address this issue, the current study attempts to reproduce the RMSL variabilities in the PRD that would have occurred in the absence of large-scale human interventions by means of a regression model. This approach allows for the isolation of the overall human impact on changes in the RMSL from the concomitant alteration by global climate change.

The paper is organized as follows. In section 2, an overview of the study area is presented. In section 3, the dataset and the methodology used in this study are shown. In section 4, the long-term trend in the RMSL is analysed, and a regression model was used to quantify the contributions made by both human interventions and global climate change to the alteration of the RMSL. Finally, the conclusions are drawn in section 5.

2. Overview of the Pearl River Delta (PRD)

The Pearl River Delta (PRD), located in southern China, ranks as Chinas third-largest delta (after the Yangtze River and Yellow River deltas) with a drainage area of $4.5 \times 10^5\,km^2$ (Fig. 1). The PRD system consists of complex river networks and outer bays, involving three major tributaries of East, North, and West rivers flowing into the South China Sea through eight outlets (Humen, Jiaomen, Hongqimen, Hengmen, Modaomen, Jitimen, Hutiaomen, and Yamen), which significantly nourishes the PRD area and brings fast socio-economic development. The three outer bays of Lingdingyang, Modaomen, and Huangmaohai, as transitional zones of land and open sea, are of primary ecological importance in estuarine and coastal management. They are generally characterized by strong physical and biogeochemical gradients, such as water level, salinity, suspended sediment and various dissolved nutrients, as a result of complex interactions between saline water and fresh water. In this study, we mainly focus on the dominant parts of the PRD, including the West River Delta and the North River Delta, which contribute approximately 92% of the water discharge delivering into the South China Sea (Zhang et al., 2015a).

The Pearl River delivers approximately $2823 \times 10^8\,m^3/yr$ of freshwater discharge and $72.4 \times 10^6\,t/yr$ of sediment load into the South China Sea (Liu et al., 2018b). There appears a strongly seasonal variation in both incoming sediment load and water discharge in the PRD, with approximately 95% of the sediment load and 80% of the water discharge being delivered during the flood season from April to September, while only 5% and 20% of these are delivered during the dry season from October to March, respectively. In particular, approximately 45–50% of the total runoff and 60% of the total suspended sediment are discharged into the South China Sea via western outlets (Yamen, Hutiaomen, Jitimen, and Modaomen), while the rest drain into the Lingdingyang Bay through eastern outlets (Hengmen, Hongqimen, Jiaomen, and Humen). The mean annual river discharge entering the PRD is approximately $8952\,m^3/s$ (Liu et al., 2014). The tidal regime in the PRD is characterized by a mixed semi-diurnal tide with a mean tidal range between 1.0 and 1.7 m near the outlets (Mao et al., 2004; Zhang et al., 2010). As tides propagate offshore and move toward the channel networks, they are influenced by various external forces, including bottom friction, river discharge and meteorological factors. Generally, the spatial pattern of the tidal regime in the PRD features three distinctive regions, i.e., the Humen estuary and Yamen estuary located in the eastern and western part, respectively, being the tide-dominated regions with a typical funnel shape, and the remaining six estuaries (i.e., Jiaomen, Hongqili, Hengmen, Modaomen, Jitimen, and Hutiaomen) being situated in the central part of the PRD, being river-dominated regions (Cai et al., 2018).

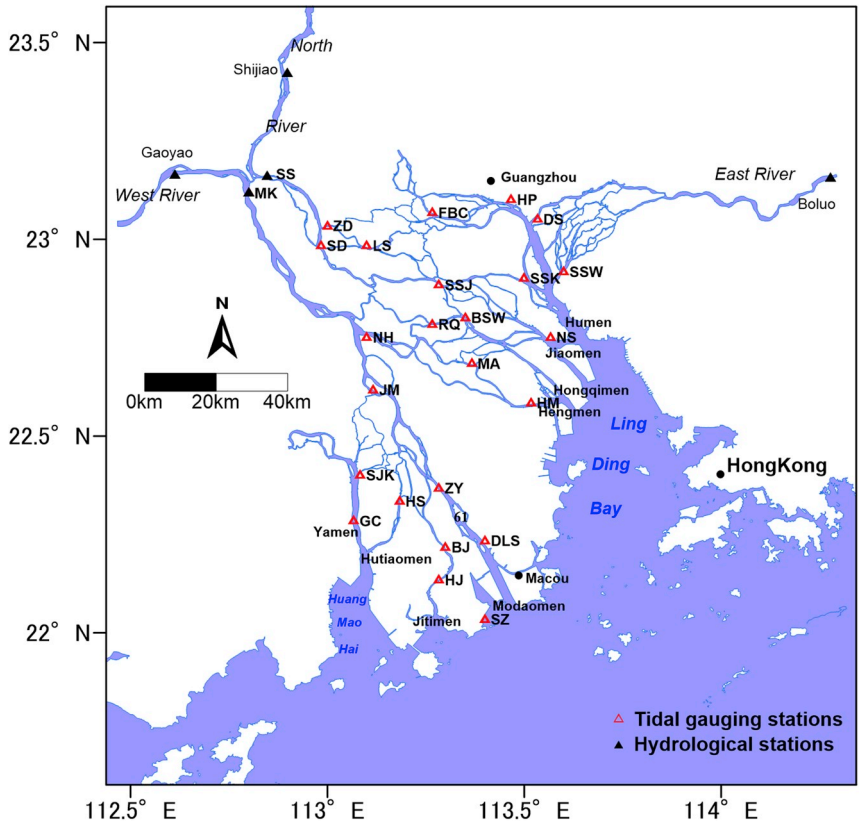

Fig. 1. Map of the Pearl River Delta displaying the tidal gauging and hydrological stations used in current study.

3. Datasets and methods

3.1. Datasets

A dataset of monthly averaged RMSL covering the 1950s-2016 from 26 gauging stations was collected in the PRD region. The data were provided by the Guangdong Hydrology Bureau of the People's Republic of China. In particular, the RMSL has been corrected using the reference local mean sea level (i.e., Zhujiang datum). The location of the gauging station is shown in Fig. 1 and their basic information can be seen in Table 1. To understand the impacts of river discharge on the RMSL, monthly averaged streamflow data were collected at the Gaoyao and Shijiao hydrological stations (see Fig. 1), which are two upstream stations controlling the fluctuations of RMSL in the PRD.

3.2. Detection of trends and change-points

In this study, non-parametric method, the Mann-Kendall test, was used to detect the trends and change-points of the studied RMSL time series in the PRD. The advantage of such a method lies in that no assumption of normality of the independent dataset is required. For a detailed description of the method, readers can refer to Appendix A.

3.3. Reconstruction of monthly averaged RMSL

A simple yet effective bivariate linear regression model was used to reconstruct the RMSL as a function of river discharge, Q, and a dimensionless normalized RMSL coefficient, S:

$$\mathrm{RMSL} = a_0 + a_1 S + a_2 Q, \quad (1)$$

where a_i ($i = 0, 1, 2$) are coefficients determined by calibration against observations. The fundamental assumption is that Q can be used as the main proxy for all processes related to the riverine forces from the catchment scale (including natural and human-induced changes), while S is introduced into the model to account for the integrated effect of marine processes (from the tide, storm surge, coastal circulation, etc.). The values of S were obtained by scaling the time series of RMSL in the

Table 1
Summary of tide gauging stations used for the assessment of human interventions from the 1950s to 2016.

Stations	Abbreviation	Longitude	Latitude	Period	Length (year)
Makou	MK	11248′	2307′	1959–2016	58
Sanshui	SS	11205′	2301′	1959–2016	58
Dasheng	DS	11332′	2303′	1956–2016	61
Sishengwei	SSW	11336′	2255′	1964–2016	53
Fubiaochang	FBC	11316′	2304′	1955–2016	62
Huangpu	HP	11328′	2306′	1955–2016	62
Jiangmen	JM	11307′	2237′	1957–2016	60
Zhuyin	ZY	11317′	2222′	1959–2016	58
Denglongshan	DLS	11324′	2214′	1959–2016	58
Sanjiangkou	SJK	11305′	2224′	1955–2016	62
Guanchong	GC	11304′	2217′	1961–2016	56
Hengshan	HS	11311′	2202′	1957–2016	60
Baijiao	BJ	11318′	2213′	1956–2016	61
Huangjin	HJ	11317′	2208′	1965–2016	52
Sanzhao	SZ	11324′	2202′	1965–2016	52
Nanhua	NH	11306′	2245′	1955–2016	62
Hengmen	HM	11331′	2235′	1955–2016	62
Maan	MA	11322′	2241′	1956–2016	61
Rongqi	RQ	11316′	2247′	1956–2016	61
Sanduo	SD	11259′	2259′	1955–2016	62
Sanshanjiao	SSJ	11317′	2253′	1955–2016	62
Banshawei	BSW	11321′	2248′	1955–2016	62
Zidong	ZD	11300′	2302′	1955–2016	62
Lanshi	LS	11306′	2259′	1955–2015	62
Sanshakou	SSK	11303′	2254′	1955–2016	62
Nansha	NS	11334′	2245′	1955–2016	62

range between 0 and 1 by using the following formula:

$$S = \frac{RMSL - RMSL_{min}}{RMSL_{max} - RMSL_{min}}, \quad (2)$$

where the subscripts 'min' and 'max' indicate the minimum and maximum RMSL, respectively. In order to represent the forcing from the ocean scale, we used the averaged time series of S of fiver gauging stations near the estuary mouth (i.e., GC, HJ, SZ, HM, NS). We have checked the seasonal difference of RMSL at these five gauging stations during the studied period (1950s-2016) and the maximum difference between wet and dry seasons is generally less than 0.14 m, which suggests a tide-dominated character and the impact of river discharge on RMSL in these stations is negligible.

The objective functions adopted for identifying the best set of model parameters were the commonly used root mean square error (RMSE) between the monthly averaged values of the simulated and observed RMSL, and the coefficient of determination R^2:

$$RMSE = \sqrt{\frac{\sum_{i=1}^{n}(RMSL_{obs,i} - RMSL_{sim,i})^2}{n}}, \quad (3)$$

$$R^2 = 1 - \frac{\sum_{i=1}^{n}(RMSL_{obs,i} - RMSL_{sim,i})^2}{\sum_{i=1}^{n}(RMSL_{obs,i} - \overline{RMSL_{obs}})^2}, \quad (4)$$

where n is the number of observations, $RMSL_{obs}$ and $RMSL_{sim}$ are the observed and simulated RMSL values, respectively, and the overbar indicates averaged value. We also tested several commonly used regression models, and the comparisons with the simple bivariate linear regression model were presented in Appendix B.

To quantify the impact of human interventions, the whole studied period was divided into two periods: the pre-HUM and post-HUM period, representing the period with and without impacts from human interventions, respectively. The pre-HUM period was used for calibration. The calibrated model was then re-run over the post-HUM period to predict the expected RMSL if there were no significant human interventions (e.g., dam constructions, dredging, sand excavation, and land reclamation), and the discharges and coefficients of the variation in mean water level were actually measured.

The total change in the RMSL in the post-HUM period relative to the pre-HUM period, including both global climate change and human interventions, is evaluated as:

$$\Delta_{TOT} = RMSL_{obs,post-HUM} - RMSL_{obs,pre-HUM}, \quad (5)$$

which represents the difference in mean RMSL between observed values for the post-HUM ($RMSL_{obs,post-HUM}$) period and those for the pre-HUM ($RMSL_{obs,pre-HUM}$) period.

This total change in the RMSL can be regarded as the combination of two effects:

1) The contribution related to changes in climate (Δ_{CLI}), defined as the difference between the RMSL values simulated for the post-HUM ($RMSL_{sim,post-HUM}$) and pre-HUM ($RMSL_{sim,pre-HUM}$) period

$$\Delta_{CLI} = RMSL_{sim,post-HUM} - RMSL_{sim,pre-HUM}. \quad (6)$$

2) The contribution ascribable to the overall impact of human interventions (Δ_{HUM}), defined as the difference between the observed ($RMSL_{obs,post-HUM}$) and simulated ($RMSL_{sim,post-HUM}$) values of RMSL for the post-HUM period

$$\Delta_{HUM} = RMSL_{obs,post-HUM} - RMSL_{sim,post-HUM}. \quad (7)$$

Combining the above equations, we obtain $\Delta_{HUM} = \Delta_{TOT} - \Delta_{CLI} + \varepsilon$, where $\varepsilon = RMSL_{sim,pre-HUM} - RMSL_{obs,pre-HUM}$ is the model bias (i.e., mean error) between the simulated and observed RMSL during the calibration period. To assess the performance of the model in estimating RMSL differences, Δ_{HUM} should be compared with the bias ε at different time scales (annual and seasonal). The confidence in the model is high if $\varepsilon \ll \Delta_{HUM}$.

Table 2
Mann-Kendall trend test results for the RMSL collected from 26 gauging stations in the PRD.

Type	Stations	β (mm/yr)	p-value	Change-point
Descending	MK	−27.18	< 0.001	1997
	SS	−23.51	< 0.001	2000
	NH	−8.05	< 0.001	1998
	JM	−9.92	< 0.001	2000
	ZY	−2.04	< 0.001	2000
	SD	−4.30	< 0.001	2000
	ZD	−5.66	< 0.001	2000
	LS	−3.54	< 0.001	1997
	BSW	−1.62	< 0.001	2007
	RQ	−1.41	< 0.001	2002
	BJ	−0.98	< 0.001	1998
Ascending	DS	1.31	< 0.001	1982
	SSW	2.77	< 0.001	1985
	HP	0.38	< 0.001	1987
	HM	3.34	< 0.001	1982
	SSK	0.42	< 0.001	1974
	NS	1.41	< 0.001	1987
	SJK	0.65	< 0.001	1973
	GC	1.72	< 0.001	1978
	HJ	1.78	< 0.001	1990
Fluctuant	SZ	0.12	0.26	–[a]
	DLS	−0.28	0.03	2008
	MA	−0.50	0.02	2002
	FBC	−0.38	0.0015	2012
	SSJ	0.10	0.67	2007
	HS	0.09	0.41	–

[a] '–' indicates that the change point is not available.

4. Results

4.1. Long-term trend of RMSL and its spatial patterns

To identify the long-term trend of RMSL and its spatial patterns over the PRD, the Mann-Kendall trend test was applied to the annual RMSL time series in 26 gauging stations in the PRD. The results are summarized in Table 2, where the positive value of magnitude in trend β indicates an increasing trend, while a negative value suggests a decreasing trend. Remarkably, we observe that most stations show either a significant increasing trend or a significant decreasing trend at a > 95% confidence level with p-value < 0.05, with the only exceptions being SZ, DLS, MA, FBC, SSJ and HS stations.

The spatial distribution of magnitude in the trend of RMSL is illustrated in Fig. 2, which reflects a cumulative impact from global climate change and human interventions. In general, the RMSL patterns in the PRD are categorized into three types: descending, ascending and fluctuant. It can be seen that most stations located in the channel networks are characterized by a significant descending trend in RMSL (defined as a descending type), with the maximum decreasing trend being around −23.51 and −27.18 mm/yr occurring at SS and MK stations situated at the apex of the PRD. In the upper and central parts of the PRD, the descending rate was gradually reduced, but most stations (e.g., the SD, ZD, LS stations in the North River and the NH, JM stations in the West River) still display a significant descending trend with β being −3.54 ~ -9.92 mm/yr. For stations located at the central and lower parts of the PRD, the descending rate is generally less than 1 mm/yr. In contrast, a general ascending tendency is detected for most stations at the outlets (defined as an ascending type), such as the HP, DS, SSW, SSK, NS, HM, HJ, GC, SJK stations, with the maximum ascending tendency detected at the HM station with β = 3.34 mm/yr. The third type

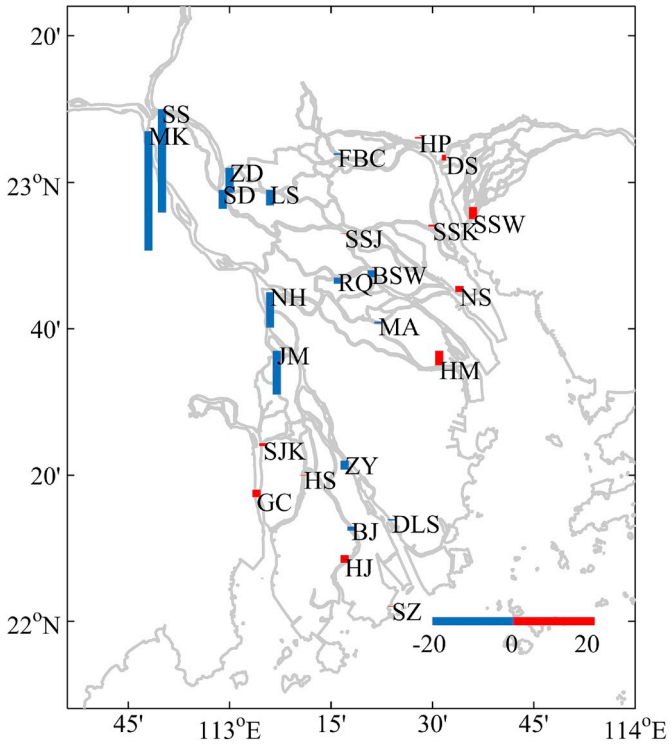

Fig. 2. Magnitude in trend β (mm/yr) obtained from Mann-Kendall trend test. The negative value indicated by the blue bar, shows a decreasing trend, while positive value indicated by the red bar, shows an increasing trend. (For interpretation of the references to colour in this figure legend, the reader is referred to the Web version of this article.)

is characterized by a fluctuant shape with either a negligible value of β (such as the SZ, DLS, MA, FBC, SSJ and HS stations) or a positive β (such as MA). Such distribution patterns in the RMSL are closely related to river-tide dynamics in the PRD. Specifically, the descending type corresponds to the upper and central parts of the channel networks being river-dominated, with a relatively high value of residual water levels, while the ascending type corresponds to the eastern and western sides being tide-dominated, with relatively low values of residual water levels (see Cai et al., 2018). To understand the relative importance of riverine and marine processes on RMSL, a bivariate regression model is used to reproduce the RMSL dynamics that would have occurred in the absence of human interventions (see discussions in section 4.3).

To illustrate changes in the RMSL in the PRD, the Mann-Kendall trend test results for some typical stations are shown in Fig. 3. Fig. 3a and b displays the results for the MK and SS stations located at the apex of the PRD, where we observe a strong descending trend for the whole study period. In the case of MK station, the Mann-Kendall trend test shows no obvious trend in the RMSL before the mid-1980s, after which a significant descending trend is detected between the mid-1980s and 2005. After 2005, the RMSL series shows no obvious trend again. For the SS station, the Mann-Kendall trend test in the RMSL shows a slightly increasing trend from 1959 to the mid-1980s, while after mid-1980s the RMSL series is dominated by a significantly decreasing trend until 2005. As with the MK station, the RMSL of the SS station reaches a relatively stable status after 2005. Fig. 3c and d shows the Mann-Kendall trend test results at two stations located near the outlets (i.e., the HM and SSW stations), where a significant ascending trend in the RMSL is detected. Generally, we observe a consistently increasing trend from the 1950s until the 2000s, with a rapid change occurring at the end of 1980s. The change-point detection of the RMSL in these two stations indicates that a regime shift occurred around mid-1980s. For the fluctuant trend type (see Fig. 3e and f for the case of the MA and SSJ stations), there exists no obvious trend (hence the small values of magnitude in this trend) for the whole study period. Specifically, we observe a sudden increase in the RMSL during the early 1990s, which is likely due to the increase of freshwater discharge into the North River networks (Luo et al., 2007).

4.2. Performance of the regression model

Section 4.1 already indicates that an RMSL regime shift occurred around 1997 at MK hydrological station, which is the major controlled station in terms of river discharge for the PRD. In addition, the change-point of 1997 was further confirmed by the fact that the relationship between the cumulative annual mean water level and cumulative annual mean water discharge significantly altered after 1997 at MK station (see Fig. 4). Therefore, to quantify the impact of human interventions on the RMSL dynamics using the proposed regression model in section 3.3, we divided the whole time series into a pre-1997 period (1950s-1997), and a post-1997 period (1997–2016). Table 3 presents the values of the root mean square error (RMSE) and the coefficient of determination (R^2) for the calibration period (the pre-1997 period). It can be seen that the proposed bivariate regression model is able to satisfactorily reproduce the RMSL dynamics, with RMSE ranging from 0.01 to 0.43 m and R^2 ranging from 0.84 to 0.99. The regression model was successively executed for the post-1997 period, maintaining identical values of the previously calibrated regression coefficients. When compared to the actual measurements, the predicted results significantly deteriorate in all of the stations distributed throughout the PRD (see Table 3). This is expected and suggests that the cumulative impact of human interventions altered the RMSL regime in the PRD. Table 3 also shows the calibrated regression coefficients a_i ($i = 0, 1, 2$) for the calibration period. Generally, we observe a relatively large value for a_1 (> 0.75) but a relatively small value for a_2 ($<10^{-5}$) for those stations with a significantly increasing trend for RMSL (mostly stations located near the outlets, e.g., the DS, SSW, GC, BJ, SZ stations), which indicates a dominant influence of marine processes over the riverine processes. In contrast, for those stations showing a significantly decreasing trend in RMSL (mostly stations located in the upper and central parts of the PRD, e.g., the MK, SS, NH, SD, ZD stations), the influence of riverine processes is much stronger than for those stations near the outlets, as seen from $a_1 < 0.7$ and $a_2 > 10^{-5}$.

4.3. Quantifying the influence of human interventions on RMSL

It is well known that the RMSL dynamics are mainly controlled by the tide-river interactions in river deltas, which are subject to substantial morphological changes due to the combined influence of natural and human-induced alternations. In the case of the PRD, the channel geometry in the channel networks has been substantially altered due to large-scale sand excavation since the 1980s, which exerts a significant influence on the RMSL dynamics (Luo et al., 2007). On the other hand, the morphological changes near the outlets can be mainly attributed to the land reclamation that overwhelmingly dominates the effects of subsidence and a reduced sediment supply (Zhang et al., 2015b; Wu et al., 2016a,b). It is important to note that many human interventions take place concurrently. Therefore, we are only able to quantify the overall impacts of human interventions in general.

The successful reproduction of the natural variation of the RMSL using the bivariate regression model provides a useful tool for quantifying the impacts of natural (i.e., changes in the meteorological forcing, here represented by Q and S_{cv}) and anthropogenic factors influencing the RMSL in the post-1997 period. In the following analysis, the values of the RMSL predicted by the bivariate regression model in the post-1997 period are used to isolate the impacts on the RMSL due solely to changes in Q and S_{cv} compared to the pre-1997 period (Δ_{CLI}, see Equation (6)) on the one hand, and due solely to the presence of intensive human interventions (Δ_{HUM}, see Equation (7)) on the other hand. The annual and seasonal statistics using Equations (5)–(7), based

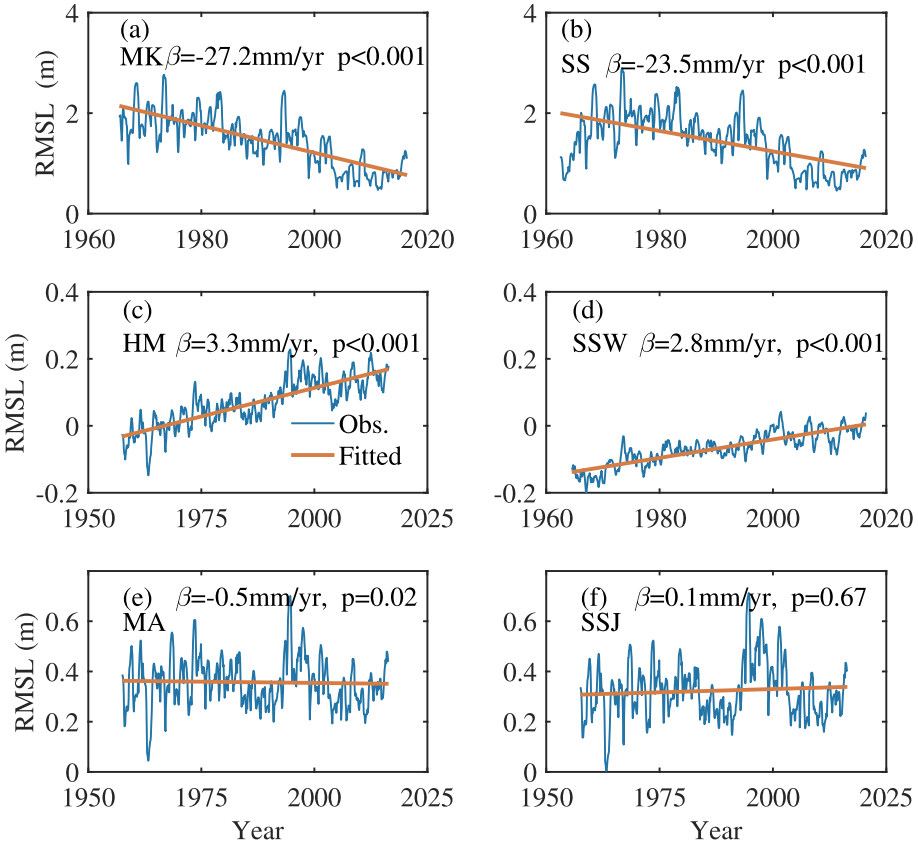

Fig. 3. Mann-Kendall trend test results at MK (a), SS (b), HM (c), SSW (d), MA (e) and SSJ (f) stations displaying a significant descending trend (a, b), a significant ascending trend (c, d) and a fluctuant trend (e, f).

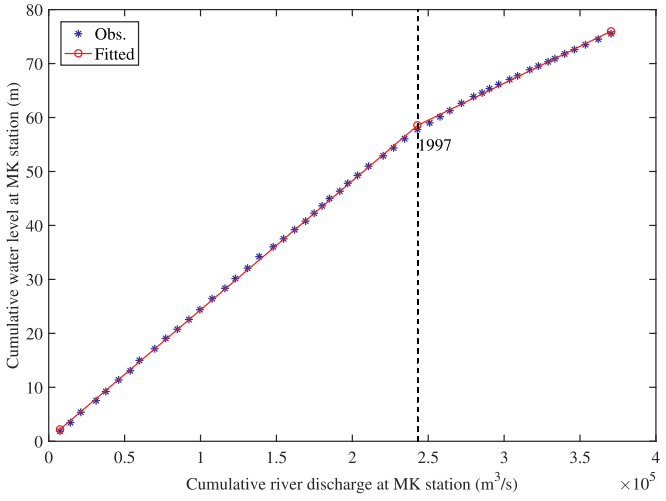

Fig. 4. Alteration in relationship between the cumulative annual mean water level and cumulative annul mean water discharge observed at MK hydrological station. The red line indicates the best linear fitting curve. (For interpretation of the references to colour in this figure legend, the reader is referred to the Web version of this article.)

on the observed and simulated RMSL for the post-1997 period, are presented in Table 4. Also listed are the seasonal (flood and dry seasons) and annual biases (ε) between simulated and observed RWT during the calibration period for each gauging station. We note that the model bias is always smaller than the computed Δ_{HUM} (ε/Δ_{HUM} being

Table 3
Performance of the bivariate regression model when applied to the 26 gauging stations in the PRD for the pre-1997 (calibration) and post-1997 periods.

Stations	Calibration (pre-1997)					Prediction (post-1997)	
	a_0	a_1	a_2	RMSE	R^2	RMSE	R^2
MK	−0.27	0.46	2.18E-04	0.32	0.95	0.55	0.16
SS	−0.17	0.31	2.14E-04	0.43	0.92	0.51	0.19
DS	−0.32	0.8	−3.46E-06	0.01	0.99	0.01	0.98
SSW	−0.36	0.82	−7.42E-06	0.03	0.95	0.02	0.91
FBC	−0.3	0.79	6.48E-06	0.02	0.98	0.04	0.81
HP	−0.32	0.79	−2.87E-06	0.02	0.96	0.02	0.95
JM	−0.1	0.72	8.05E-05	0.14	0.95	0.2	0.2
ZY	−0.22	0.8	2.21E-05	0.05	0.97	0.07	0.5
DLS	−0.24	0.81	1.07E-07	0.03	0.95	0.05	0.6
SJK	−0.26	0.79	−3.36E-06	0.04	0.91	0.04	0.87
GC	−0.26	0.81	−7.22E-06	0.04	0.9	0.05	0.79
HS	−0.31	0.8	1.20E-05	0.05	0.95	0.03	0.9
BJ	−0.25	0.79	4.38E-06	0.06	0.89	0.04	0.75
HJ	−0.3	0.88	−7.04E-06	0.03	0.93	0.04	0.86
SZ	−0.31	0.86	−1.66E-05	0.04	0.84	0.05	0.66
NH	−0.21	0.64	1.04E-04	0.16	0.96	0.23	0.47
HM	−0.3	0.8	2.57E-06	0.04	0.93	0.03	0.73
MA	−0.26	0.74	4.16E-05	0.05	0.98	0.07	0.93
RQ	−0.3	0.73	4.93E-05	0.06	0.98	0.1	0.86
SD	−0.28	0.6	1.05E-04	0.17	0.95	0.18	0.85
SSJ	−0.29	0.73	3.98E-05	0.07	0.96	0.07	0.95
BSW	−0.29	0.73	3.31E-05	0.04	0.98	0.08	0.76
ZD	−0.26	0.69	1.07E-04	0.24	0.91	0.17	0.81
LS	−0.32	0.52	8.46E-05	0.16	0.94	0.16	0.84
SSK	−0.3	0.77	−3.53E-06	0.02	0.97	0.03	0.91
NS	−0.27	0.76	−1.10E-06	0.04	0.91	0.04	0.88

Table 4
Seasonal and annual variations of the RMSL in the post-1997 period relative to the pre-1997 period caused by climate change Δ_{CLI} and human interventions Δ_{HUM}.

Stations	Flood season				Dry season				Annual			
	Δ_{TOT}	Δ_{CLI}	Δ_{HUM}	ε	Δ_{TOT}	Δ_{CLI}	Δ_{HUM}	ε	Δ_{TOT}	Δ_{CLI}	Δ_{HUM}	ε
MK	−1.28	−0.81	−0.45	0.042	−0.3	−0.19	−0.14	0.019	−0.78	−0.49	−0.29	0.041
SS	−1.2	−0.74	−0.43	0.11	−0.32	−0.2	−0.15	0.047	−0.75	−0.46	−0.29	0.086
DS	0.03	0.09	−0.06	0.004	0.05	0.12	−0.07	0.003	0.04	0.11	−0.07	0.003
SSW	0.06	0.06	0	0.012	0.08	0.09	−0.01	0.005	0.08	0.08	−0.01	0.009
FBC	−0.04	−0.03	−0.01	0.013	0	0.03	−0.03	0.006	−0.02	0	−0.02	0.01
HP	0.01	0.03	−0.03	0.004	0.02	0.06	−0.04	0.002	0.02	0.05	−0.03	0.003
JM	−0.59	−0.39	−0.21	0.043	−0.22	−0.15	−0.07	0.01	−0.4	−0.26	−0.14	0.03
ZY	−0.16	−0.05	−0.1	0.021	−0.01	0.04	−0.06	0.009	−0.08	0	−0.08	0.016
DLS	−0.06	0	−0.06	0.02	−0.02	0.03	−0.05	0.01	−0.04	0.02	−0.05	0.015
SJK	0	0.06	−0.05	0.016	0.04	0.09	−0.06	0.016	0.02	0.08	−0.06	0.019
GC	0.04	0.12	−0.07	0.012	0.06	0.14	−0.09	0.01	0.05	0.13	−0.08	0.013
HS	−0.05	0.05	−0.09	0.018	0.02	0.1	−0.09	0.014	−0.01	0.08	−0.09	0.019
BJ	−0.06	−0.02	−0.04	0.021	0.01	0.04	−0.04	0.018	−0.02	0.02	−0.04	0.018
HJ	0.03	0.08	−0.05	0.018	0.06	0.11	−0.05	0.01	0.05	0.1	−0.05	0.014
SZ	−0.01	−0.03	0.01	0.02	0	−0.01	0.02	0.011	0	−0.02	0.02	0.018
NH	−0.51	−0.35	−0.16	0.039	−0.1	−0.03	−0.06	0.004	−0.3	−0.18	−0.11	0.027
HM	0.08	0.1	−0.02	0.016	0.11	0.14	−0.03	0.006	0.1	0.12	−0.02	0.011
MA	−0.08	0.01	−0.1	0.02	0.04	0.11	−0.06	0.007	−0.02	0.06	−0.08	0.016
RQ	−0.13	−0.02	−0.12	0.019	0.04	0.12	−0.07	0.006	−0.04	0.05	−0.1	0.017
SD	−0.29	−0.25	−0.06	0.03	0	0.03	−0.02	0.013	−0.14	−0.1	−0.04	0.031
SSJ	−0.03	0.1	−0.14	0.019	0.05	0.15	−0.09	0.007	0.01	0.12	−0.11	0.021
BSW	−0.13	−0.02	−0.12	0.017	0	0.06	−0.05	0.011	−0.06	0.02	−0.08	0.016
ZD	−0.35	−0.21	−0.15	0.051	−0.07	0.02	−0.08	0.024	−0.2	−0.09	−0.11	0.038
LS	−0.2	−0.17	−0.07	0.023	0.03	0.09	−0.03	0.013	−0.08	−0.03	−0.05	0.037
SSK	0.01	0.07	−0.07	0.009	0.03	0.1	−0.07	0.005	0.02	0.09	−0.07	0.007
NS	0.05	0.12	−0.06	0.011	0.06	0.15	−0.09	0.01	0.06	0.13	−0.08	0.01

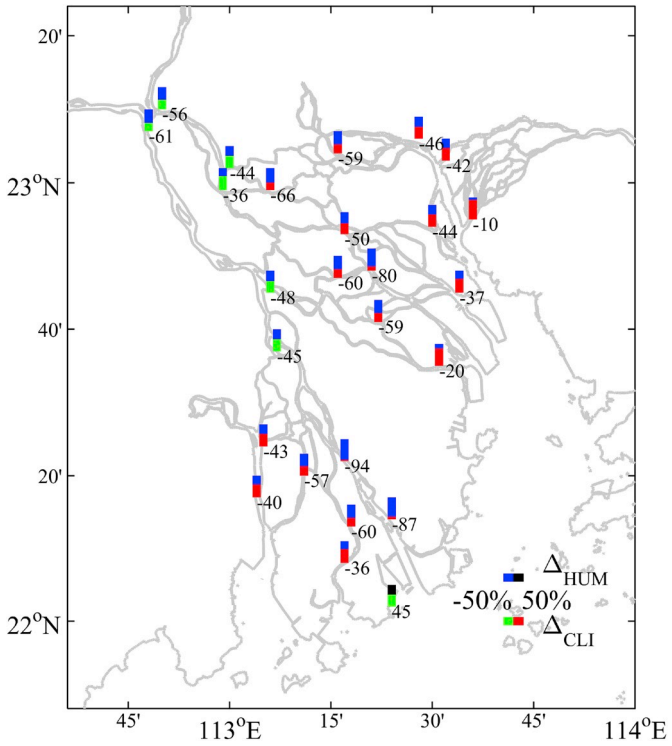

Fig. 5. Relative contributions made by human interventions (Δ_{HUM}) and climate change (Δ_{CLI}) to the alterations of RMSL in the PRD on annual scale. The labelled number indicates the contribution made by human interventions Δ_{HUM} (%).

31% and 38% at seasonal and annual scales, on average), thus suggesting that the effects of model errors on the results of the present analysis are minor.

Fig. 5 shows the contributions made by both climate change and human interventions to the alteration of the RMSL based on the annual RMSL statistics. We observe that the annual changes of the RMSL in the upper and central parts of the PRD are mainly driven by human interventions (Δ_{HUM}), with the maximum alternations occurring at the MK and SS stations. Conversely, the RMSL alterations near the estuarine outlets (e.g., the DS, SSW, HM, SZ, BJ and GC stations) are mainly determined by changes in meteorological forces (Δ_{CLI}), suggesting a diminishing effect of riverine impact with increasing distance downstream.

5. Discussions

5.1. Seasonal variability of human interventions on RMSL

When looking at the seasonal variability of Δ_{HUM} at the MK and SS stations, the noticeable alterations caused by human intervention in the flood season are −0.45 m and −0.43 m, respectively, which is much larger than those during the dry season, with Δ_{HUM} being −0.14 m and −0.15 m, respectively (Fig. 6). This means that the magnitude of human interventions in the upper and central parts of the PRD is strongly related to river discharge. To disentangle the underlying mechanisms causing the differential response of the RMSL during the year, we further present the observed RMSL and simulated Δ_{HUM} as a function of river discharge, Q, entering the PRD (Figs. 7–9).

For the first type, characterized by a significantly descending RMSL (Fig. 7), we observe that the RMSL increased with river discharge due to the strongly nonlinear residual frictional effect in river-dominated channels (Cai et al., 2018). Remarkably, the alternation caused by human interventions, Δ_{HUM}, also significantly increases with river discharge. In the case of the MK and SS stations located in the upper region of the PRD, the simulation results show that the value of Δ_{HUM} changes from −2 m for a given Q at approximately 20000 m^3/s to −5 m for a given Q at approximately 45000 m^3/s. The underlying mechanism can be explained by using the classical hydraulic geometry relation for water depth $h = cQ^b = c(AU)^b$, where b and c are coefficients, while A and U represent cross-sectional area and velocity, respectively. Here, human interventions (especially sand excavations) result in a substantial increase in cross-sectional area, A, by deepening the riverbed.

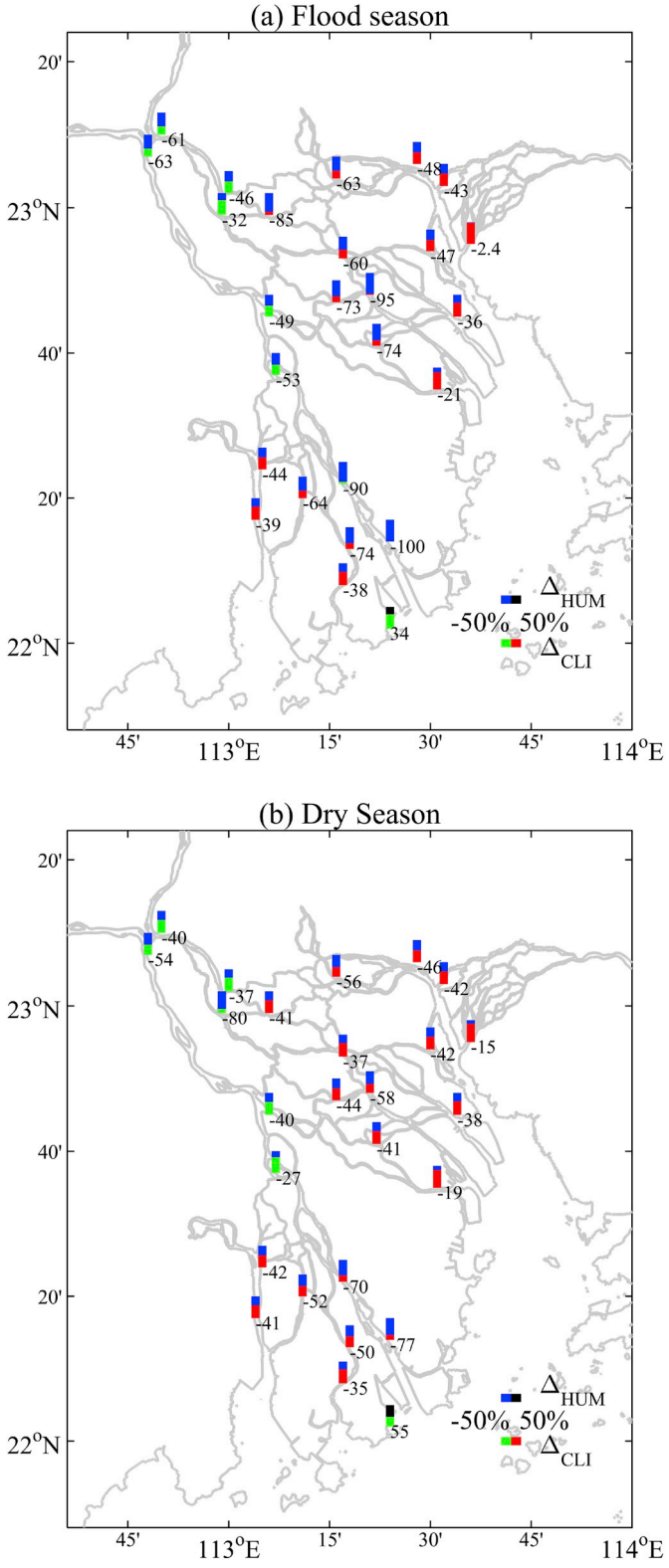

Fig. 6. Relative contributions made by human interventions (Δ_{HUM}) and climate change (Δ_{CLI}) to the alterations of RMSL in the PRD during the flood season (a) and the dry season (b). The labelled number indicates the contribution made by human interventions Δ_{HUM} (%).

For low flow conditions, the alteration of h caused by the increase of A is relatively minor due to the constraint of the low value of U. In contrast, the value of U is significantly increased for a large value of Q (e.g., > 20000 m^3/s), thus the alteration of h is much larger for the same cross-sectional area following the hydraulic geometry relation. Similarly, for stations located in the central parts of the PRD (e.g., the NH, JM, SD, and ZD stations), the alteration of Δ_{HUM} also displayed an upward tendency with Q, although the magnitude is substantially reduced compared with the MK and SS stations that are located in the upper parts of the PRD. It can be seen from Fig. 7 that the alteration of Δ_{HUM} in NH, JM, SD, ZD stations is larger than 1 m when Q exceeds 20000 m^3/s.

For the typical ascending type (Fig. 8), there exists no strong relationship between Δ_{HUM} and Q, which indicates a minor impact of Q on the alteration of the RMSL. Unlike the descending type, which is mainly influenced by the deepening caused by sand excavation, the ascending type (mostly stations located near the outlets of the PRD, e.g., the DS, SSW, HM, NS, GC, HJ stations) is mainly impacted by channel extension due to large-scale land reclamations. The fluctuant type can be regarded as a transitional type between the descending and ascending types. It can be seen from Fig. 9 that the alteration of Δ_{HUM} increases with Q but does not change as significantly as those stations categorized as descending types (generally the value of Δ_{HUM} ranges −0.2-0 m).

5.2. Implications for other river deltas

The results obtained from this study are of clear relevance to other river deltas that are subjected to intensive human activities, such as the Rhine-Meuse Delta (Vellinga et al., 2014), the Ebro Delta (Sayol and Marcos, 2018), the Mississippi River Delta (Blum and Roberts, 2009), the Nile River Delta (Susnik et al., 2015), the Mekong Delta (Dang et al., 2018), the Yangtze River Delta (Wang et al., 2018b). In all cases, it is argued that the anthropogenic interventions (e.g., accelerated land subsidence resulting from groundwater and hydrocarbon extraction, sediment trapping due to dam construction) increase the RMSL rise rates within deltas (e.g., Wolinsky et al., 2010), which is indeed the case from a physical point of view. However, the impacts of substantial deepening due to channel dredging or sand excavation on the rate of RMSL receive much less attention than other human activities since they are regarded as local issue. Remarkably, the sand excavation over all the PRD have caused dramatic riverbed degradation, with 0.59–1.73 m, 0.34–4.43 m, and 1.77–6.48 m deepening on average in the West River, North River and East River, respectively (Luo et al., 2007). Our study demonstrates that the effect of riverbed deepening on RMSL may overwhelm the compound effect of global sea level rise and land subsidence, leading to a decline of RMSL in the upper and central regions of the PRD. Hence, systematic assessment of the various human interventions on RMSL change is required for sustainable delta management.

5.3. Limitation of the regression model

The success of adopting a simple bivariate linear regression model linking the monthly averaged RMSL to river discharge in the upstream boundary and dimensionless RMSL imposed at the seaward boundary suggests an almost linear relationship between them on a monthly scale. However, tide-river interplay in river deltas is highly nonlinear (e.g., Hoitink et al., 2017), which indicates that the linear regression model is often inappropriately used to model the dynamics of RMSL in a finer scale (e.g., daily or weekly scale). In addition, linear regression model requires that the adopted multiple predictors should be independent. This means that the imposed seaward boundary condition (dimensionless RMSL averaged near the estuary mouth) should not be affected by the upstream river discharge conditions. In our case, this requirement may be not satisfied during the flood season when the river discharge dominates the whole delta. This limitation is partially compensated by using the averaged value of dimensionless RMSL near the estuary mouth. Moreover, it is worth noting that the adopted boundary conditions are assumed to be reprehensive of the natural processes. However, in real delta system both of them are subjected to human

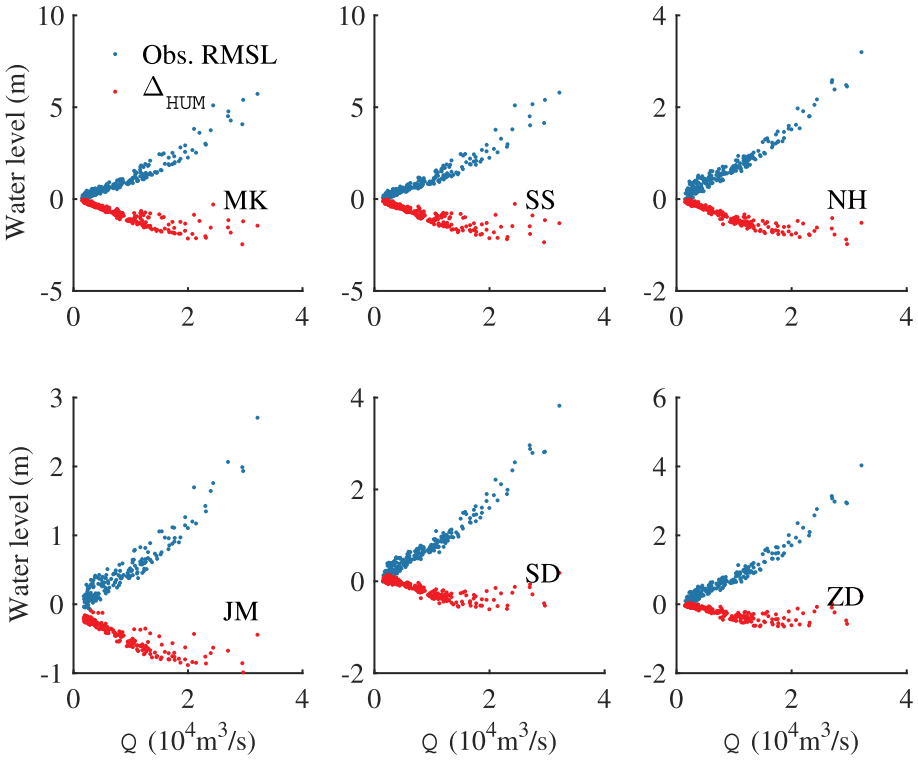

Fig. 7. Variation of the RMSL and the alteration of RMSL caused by human interventions Δ_{HUM} as a function of river discharge Q (representing by the sum of river discharge at Gaoyao and Shijiao hydrological stations) for the descending type in RMSL.

interventions from the catchment (e.g., land use/cover change, dam construction) and marine (e.g., dredging for navigational channel, land reclamations) sides. Therefore, the proposed linear regression model is preferably applied to investigate the human interventions constrained to the boundaries.

6. Conclusions

In this study, we examined the changes in the RMSL under the combined effects of the natural and human-induced changes to the PRD, with the specific aim of quantifying the separate effects of climate

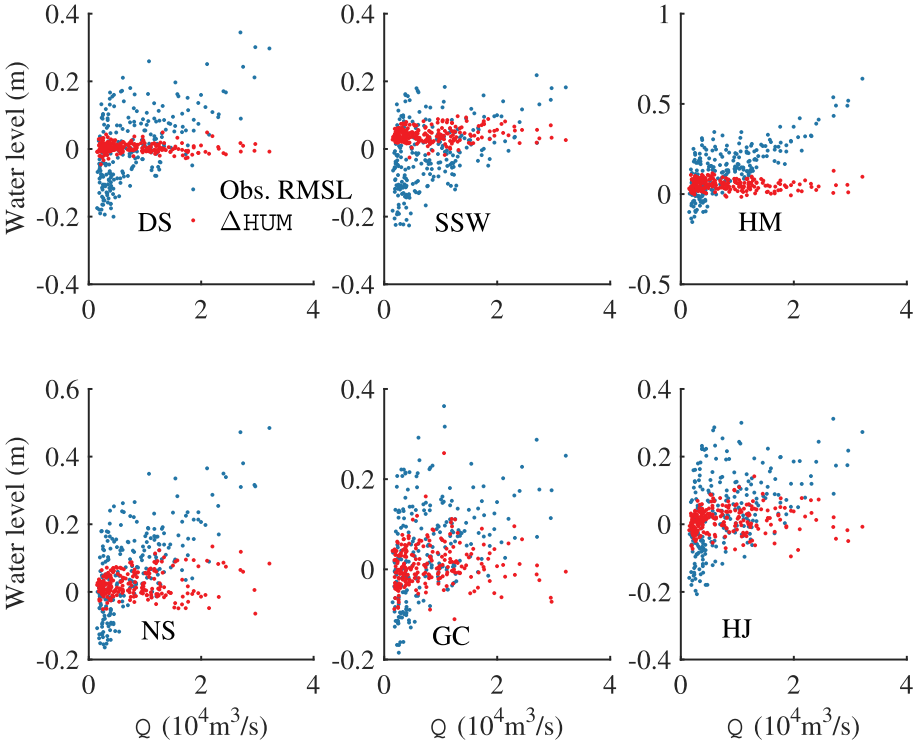

Fig. 8. Variation of the RMSL and the alteration of RMSL caused by human interventions Δ_{HUM} as a function of river discharge Q (representing by the sum of river discharge at Gaoyao and Shijiao hydrological stations) for the ascending type in RMSL.

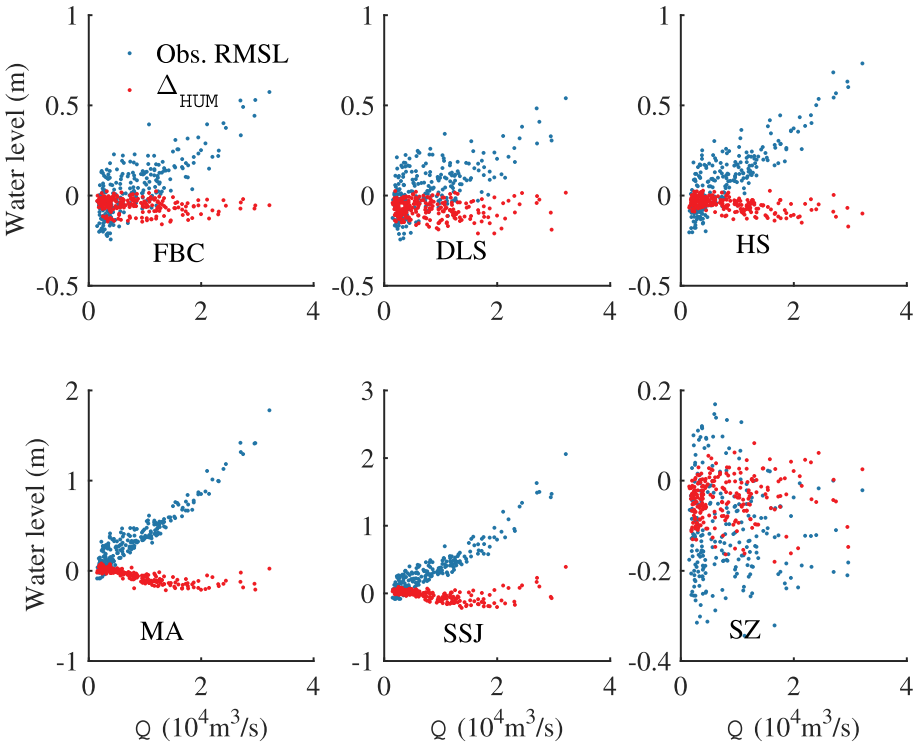

Fig. 9. Variation of the RMSL and the alteration of RMSL caused by human interventions Δ_{HUM} as a function of river discharge Q (representing by the sum of river discharge at Gaoyao and Shijiao hydrological stations) for the fluctuant type in RMSL.

change and human interventions. Based on the recorded data from 26 stations during the 1950s-2016, the spatial-temporal patterns of the RMSL were investigated by means of the Mann-Kendall trend test. To further quantify the separate effects of climate change and human interventions on the dynamics of the RMSL, a simple bivariate linear regression model is used to reconstruct the potential RMSL due solely to changes in riverine (represented by upstream river discharge) and marine (represented by the dimensionless normalized RMSL coefficient averaged near the outlets) processes. By doing so, it is possible to quantify the alterations induced by the presence of large-scale human interventions, such as sand excavation in the channel networks and land reclamations near the outlets.

It was shown that the RMSL dynamics can be categorized by three distinct types, descending, ascending and fluctuant, depending on the relative influence of riverine and marine processes. Because most stations located in the upper and central parts of the PRD are river-dominated, the RMSL displays a significantly descending tendency due primarily to substantial deepening from large-scale sand excavation occurring in the channel networks. In contrast, because most stations near the outlets are tide-dominated, we observe an upward tendency for the study period due to the combined influences of rising global sea levels and land reclamations. The third type is characterized by a fluctuant variation in the RMSL with more or less the same influence from riverine and marine processes.

Unlike our previous study using an analytical approach to understand the nonlinear tide-river interactions in estuaries (Cai et al., 2018), for the first time, a simple yet effective bivariate regression model was used to quantify the cumulative effects of human interventions on the RMSL dynamics. The simulated results confirm our analysis regarding the potential impacts from human interventions on the PRD, with the most intensive human-induced impacts occurring in the upper and central parts of the PRD. Moreover, we also identify seasonal changes in the RMSL caused by human interventions, which suggests a stronger impact during the flood season. These findings will be beneficial for general water resources management in complex river deltas.

Acknowledgment

We acknowledge the financial support from the National Key R&D of China (Grant No. 2016YFC0402601), from the National Natural Science Foundation of China (Grant No. 51709287, 41106015, 41476073), from the Basic Research Program of Sun Yat-Sen University (Grant No. 17lgzd12), from the Water Resource Science and Technology Innovation Program of Guangdong Province (Grant No. 2016–20), and from the Guangdong Provincial Natural Science Foundation of China (Grant No. 2017A030310321).

Appendix A. Mann-Kendall trend test and change-point detection

The Mann-Kendall trend test, originally proposed by Mann (1945) and Kendall (1975), is a non-parametric method. The null hypothesis, H_0, of the Mann-Kendall trend test indicates that the data come from a population with independent realizations and are identically distributed. The alternative hypothesis, H_A, shows that the data had a monotonic trend. The test statistics of the Mann-Kendall trend method can be expressed as follows:

$$S = \sum_{k=1}^{n-1} \sum_{j=k+1}^{n} \mathrm{sgn}(x_j - x_k)\,, \tag{A.1}$$

where S is the statistics of the Mann-Kendall test, x_j and x_k are the jth and kth value of the dataset, respectively, n is the total number of the dataset, and sgn(.) is the index, defined as:

$$\mathrm{sgn}(x) = \begin{cases} 1 & \text{if } x > 0 \\ 0 & \text{if } x = 0 \\ -1 & \text{if } x < 0 \end{cases}. \tag{A.2}$$

The variance σ^2 is given by

$$\sigma^2 = \left\{ n(n-1)(2n+5) - \sum_{j=1}^{p} t_j(t_j-1)(2t_j+5) \right\} / 18 , \tag{A.3}$$

where p is the number of the tied groups in the dataset, t_j is the number of data points in the jth tide group. The statistic S is approximately normally distributed, provided that there is a Z-transformation in the following formula:

$$Z = \begin{cases} \frac{S-1}{\sigma} & \text{if } S > 0 \\ 0 & \text{if } S = 0 \\ \frac{S+1}{\sigma} & \text{if } S < 0 \end{cases}. \tag{A.4}$$

The indicator for measuring trend size is computed by the following expression:

$$\beta = \mathrm{Median}\left(\frac{x_i - x_j}{i-j} \right) \text{for all } 1 \le j < i \le n , \tag{A.5}$$

where β represents the magnitude of slope, with a positive value indicating a rising trend and a negative value representing a declining trend. The Mann-Kendall trend test is shown as follows: Null hypothesis H_0: $\beta = 0$; when $|Z| > Z_{1-\alpha/2}$, reject the null hypothesis (H_0), where $\mp Z_{1-\alpha/2}$ is the standard normal variance and α is the significant test level.

For a given unstable and noncontinuous varying process, the Mann-Kendall change-point detection method is a commonly used approach to detect change-point. The implementation steps of the Mann-Kendall change-point detection method are as follows:

(I) For a time series x with n sample size, a rank sequence is constructed.

$$R_k = \sum_{i=1}^{k} r_i (k = 2,3,\ldots,n) , \tag{A.6}$$

where

$$r_i = \begin{cases} 1 & x_i > x_j \\ 0 & x_i \le x_j \end{cases} (j = 1,2,\ldots,i) , \tag{A.7}$$

and R_k is the cumulative number when the ith value is greater than the jth value.

(II) Under the assumption of the random independence of time series, statistics UF_k are defined as:

$$UF_k = \frac{[R_k - E(R_k)]}{\sqrt{\mathrm{Var}(R_k)}} , \tag{A.8}$$

$$E(R_k) = \frac{n(n-1)}{4} , \tag{A.9}$$

$$\mathrm{Var}(R_k) = \frac{n(n-1)(2n+5)}{72} , \tag{A.10}$$

where $UF_1 = 0$. Statistic R_k, which is a statistic sequence calculated in sequence of time series x, obeys standard normal distribution. For a given significant level α, If $UF_k > UF_\alpha$ through looking up the normal distribution table, then this indicates that there is a significant trend change in the sequence x.

(III) The method stated in (II) is applied to the reverse sequence of time series, according to x_n, x_{n-1}, …, x_1, and the above process is repeated,

$$UB_k = -UF_k , \tag{A.11}$$

(IV) Given the significant level of α, the two statistics curves of UF_k and UB_k and the significant horizontal lines are shown on the same graph. If both values are greater than 0, then the sequence shows an upward trend; it shows a downward trend when both values of UF_k and UB_k are less than 0. When the values of UF_k and UB_k exceed the critical line, this indicates that the upward or downward trend is significant, and the range beyond the boundary line is identified as a time domain of change-point. If the curves of UF_k and UB_k have intersection points, and the intersection point is between critical lines, then the corresponding point of intersection is the time of mutation initiation.

Appendix B. Regression models for estimating the monthly averaged RMSL

To identify the best regression model for reproducing the monthly averaged RMSL as a function of river discharge, Q, and the coefficient of variation in the mean water level, S, we tested several regression models typically used in the literature:

1) Bivariate linear regression model

$$RMSL = a_0 + a_1 S + a_2 Q , \tag{B.1}$$

2) Power regression model

$$RMSL = a_0 S^{a_1} Q^{a_2}\ , \tag{B.2}$$

3) Exponential regression model

$$RMSL = a_0 e^{a_1 S} e^{a_2 Q}\ , \tag{B.3}$$

4) Logistic regression model

$$RMSL = \frac{1}{1 + e^{a_1 S e^{a_2 Q}}}\ , \tag{B.4}$$

5) Power-based polynomial regression model

$$RMSL = a_0 + a_1 S^{\beta} + a_2 Q^{\gamma}\ , \tag{B.5}$$

where a_i ($i = 0, 1, 2$) and β, γ in equation (B.5) are coefficients determined by calibration against observations. The values of RMSE and R^2 of the regression models are displayed in Table 1, where we observe that the bivariate linear regression model and power-based polynomial regression model perform better compared with other regression models. For simplification, in this study we adopted the bivariate linear regression model for reproducing the RMSL.

Table B.1
Assessment of different regression models using RMSE and R^2

Stations	RMSE (m)					R^2				
	Eq. (1)	Eq. (2)	Eq. (3)	Eq. (4)	Eq. (5)	Eq. (1)	Eq. (2)	Eq. (3)	Eq. (4)	Eq. (5)
MK	0.35	0.41	1.91	1.18	0.35	0.94	0.88	0.34	0.86	0.94
SS	0.40	0.48	2.07	1.19	0.40	0.93	0.83	0.10	0.87	0.93
DS	0.01	0.03	0.03	0.10	0.01	0.99	0.75	0.06	0.22	0.99
SSW	0.02	0.03	0.03	0.10	0.02	0.95	0.66	0.10	0.16	0.95
FBC	0.02	0.03	0.05	0.15	0.02	0.98	0.83	0.09	0.41	0.98
HP	0.02	0.03	0.04	0.10	0.02	0.96	0.74	0.09	0.23	0.96
JM	0.16	0.17	0.51	0.58	0.16	0.93	0.92	0.68	0.78	0.93
ZY	0.05	0.06	0.13	0.25	0.05	0.96	0.91	0.26	0.60	0.96
DLS	0.03	0.04	0.05	0.14	0.03	0.95	0.81	0.13	0.29	0.95
SJK	0.04	0.04	0.05	0.10	0.03	0.91	0.78	0.17	0.21	0.92
GC	0.04	0.04	0.05	0.09	0.04	0.89	0.70	0.18	0.21	0.90
HS	0.05	0.05	0.10	0.19	0.04	0.95	0.93	0.24	0.49	0.96
BJ	0.04	0.04	0.06	0.15	0.04	0.94	0.82	0.14	0.36	0.94
HJ	0.03	0.04	0.04	0.10	0.03	0.92	0.68	0.14	0.22	0.92
SZ	0.04	0.06	0.05	0.10	0.04	0.82	0.41	0.20	0.46	0.83
NH	0.18	0.19	0.67	0.68	0.18	0.94	0.95	0.79	0.84	0.94
HM	0.03	0.04	0.05	0.16	0.03	0.95	0.81	0.12	0.39	0.95
MA	0.05	0.06	0.18	0.36	0.04	0.98	0.87	0.24	0.77	0.99
RQ	0.06	0.08	0.20	0.40	0.05	0.98	0.84	0.24	0.78	0.99
SD	0.18	0.19	0.52	0.79	0.16	0.95	0.82	0.47	0.98	0.96
SSJ	0.07	0.09	0.15	0.34	0.05	0.96	0.76	0.18	0.71	0.98
BSW	0.05	0.06	0.14	0.32	0.04	0.98	0.84	0.19	0.73	0.98
ZD	0.26	0.25	0.62	0.82	0.25	0.90	0.84	0.59	0.89	0.90
LS	0.14	0.18	0.31	0.58	0.11	0.95	0.70	0.25	0.87	0.97
SSK	0.02	0.03	0.03	0.10	0.02	0.97	0.72	0.08	0.20	0.97
NS	0.04	0.04	0.05	0.12	0.04	0.92	0.75	0.13	0.35	0.92
Average	0.09	0.11	0.31	0.35	0.09	0.94	0.79	0.24	0.53	0.95

References

Blum, M.D., Roberts, H.H., 2009. Drowning of the Mississippi delta due to insufficient sediment supply and global sea-level rise. Nat. Geosci. 2, 488–491. https://doi.org/10.1038/ngeo553.

Buschman, F.A., Hoitink, A.J.F., van der Vegt, M., Hoekstra, P., 2009. Subtidal water level variation controlled by river flow and tides. Water Resour. Res. 45. https://doi.org/10.1029/2009WR008167.

Cai, H., Savenije, H.H.G., Jiang, C., 2014a. Analytical approach for predicting fresh water discharge in an estuary based on tidal water level observations. Hydrol. Earth Syst. Sci. 18, 4153–4168. https://doi.org/10.5194/hess-18-4153-2014.

Cai, H., Savenije, H.H.G., Jiang, C., Zhao, L., Yang, Q., 2016. Analytical approach for determining the mean water level profile in an estuary with substantial fresh water discharge. Hydrol. Earth Syst. Sci. 20, 1177–1195. https://doi.org/10.5194/hess-20-1177-2016.

Cai, H., Savenije, H.H.G., Toffolon, M., 2014b. Linking the river to the estuary: influence of river discharge on tidal damping. Hydrol. Earth Syst. Sci. 18, 287–304. https://doi.org/10.5194/hess-18-287-2014.

Cai, H., Yang, Q., Zhang, Z., Guo, X., Liu, F., Ou, S., 2018. Impact of river-tide dynamics on the temporal-spatial distribution of residual water levels in the Pearl River channel networks. Estuar. Coasts 1. https://doi.org/10.1007/s12237-018-0399-2.

Cazenave, A., Dieng, H.B., Meyssignac, B., Schuckmann, K.V., Decharme, B., Berthier, E., 2014. The rate of sea-level rise. Nat. Clim. Change 4, 358–361. https://doi.org/10.1038/NCLIMATE2159.

Cazenave, A., Henry, O., Munier, S., Delcroix, T., Gordon, A.L., Meyssignac, B., Llovel, W., Palanisamy, H., Becker, M., 2012. Estimating ENSO influence on the global mean sea level, 1993-2010. Mar. Geodes. 35, 82–97. https://doi.org/10.1080/01490419.2012.718209.

Church, J.A., White, N.J., 2006. A 20th century acceleration in global sea-level rise. Geophys. Res. Lett. 33, L01602. https://doi.org/10.1029/2005GL024826.

Church, J.A., White, N.J., 2011. Sea-level rise from the late 19th to the early 21st century. Surv. Geophys. 32, 585–602. https://doi.org/10.1007/s10712-011-9119-1.

Church, J.A., Clark, P.U., Cazenave, A., Gregory, J.M., Jevrejeva, S., Levermann, A.,

Unnikrishnan, A.S., 2013. Sea level change. In: Stocker, T.F. (Ed.), Climate Change 2013: the Physical Science Basis. Contribution of Working Group I to the Fifth Assessment Report of the Intergovernmental Panel on Climate Change. Cambridge University Press, Cambridge, UK, pp. 1137–1216.
Dang, T.D., Cochrane, T.A., Arias, M.E., Tri, V.P.D., 2018. Future hydrological alterations in the Mekong Delta under the impact of water resources development, land subsidence and sea level rise. J. Hydrol. Reg. Stud. 15, 119–133. https://doi.org/10.1016/j.ejrh.2017.12.002.
Day, J.W., Agboola, J., Chen, Z.Y., D'Elia, C., Forbes, D.L., Giosan, L., Kemp, P., Kuenzer, C., Lane, R.R., Ramachandran, R., Syvitski, J., Yanez-Arancibia, A., 2016. Approaches to defining deltaic sustainability in the 21st century. Estuar. Coast. Shelf Sci. 183, 275–291. https://doi.org/10.1016/j.ecss.2016.06.018.
Du, J., Shen, J., Zhang, Y.L.J., Ye, F., Liu, Z., Wang, Z., Wang, Y., Yu, X., Sisson, M., Wang, H.V., 2018. Tidal response to sea-level rise in different types of estuaries: the importance of length, bathymetry, and geometry. Geophys. Res. Lett. 45, 227–235. https://doi.org/10.1002/2017GL075963.
Ericson, J.P., Vorosmarty, C.J., Dingman, S.L., Ward, L.G., Meybeck, M., 2006. Effective sea-level rise and deltas: causes of change and human dimension implications. Glob. Planet. Chang. 50, 63–82. https://doi.org/10.1016/j.gloplacha.2005.07.004.
Godin, G., Martinez, A., 1994. Numerical experiments to investigate the effects of quadratic friction on the propagation of tides in a channel. Cont. Shelf Res. 14, 723–748. https://doi.org/10.1016/0278-4343(94)90070-1.
Hinkel, J., Lincke, D., Vafeidis, A.T., Perrette, M., Nicholls, R.J., Tol, R.S.J., Marzeion, B., Fettweis, X., Ionescu, C., Levermann, A., 2014. Coastal flood damage and adaptation costs under 21st century sea-level rise. Proc. Natl. Acad. Sci. U. S. A 111, 3292–3297. https://doi.org/10.1073/pnas.1222469111.
Hoitink, A.J.F., Jay, D.A., 2016. Tidal river dynamics: implications for deltas. Rev. Geophys. 54, 240–272. https://doi.org/10.1002/2015RG000507.
Hoitink, A.J.F., Wang, Z.B., Vermeulen, B., Huismans, Y., Kästner, K., 2017. Tidal controls on river delta morphology. Nat. Geosci. 10, 637–645. https://doi.org/10.1038/ngeo3000.
IPCC, 2014. Summary for policymakers. In: Field, C.P. (Ed.), Climate Change 2014: Impacts, Adaptation, and Vulnerability. Part A: Global and Sectoral Aspects. Contribution of Working Group II to the Fifth Assessment Report of the Intergovernmental Panel on Climate Change. Cambridge University Press, Cambridge, United Kingdom and New York, pp. 1–32.
Kendall, M.G., 1975. Rank Correlation Methods. Griffin, London.
Liu, B.J., Peng, S.H., Liao, Y.Y., Long, W.L., 2018a. The causes and impacts of water resources crises in the Pearl River Delta. J. Clean. Prod. 177, 413–425. https://doi.org/10.1016/j.jclepro.2017.12.203.
Liu, F., Hu, S., Guo, X., Luo, X., Cai, H., Yang, Q., 2018b. Recent changes in the sediment regime of the Pearl River (South China): causes and implications for the Pearl River Delta. Hydrol. Process. 32, 1771–1785. https://doi.org/10.1002/hyp.11513.
Liu, F., Yuan, L., Yang, Q., Ou, S., Xie, L., Cui, X., 2014. Hydrological responses to the combined influence of diverse human activities in the Pearl River Delta, China. Catene 113, 41–55. https://doi.org/10.1016/j.catena.2013.09.003.
Llovel, W., Becker, M., Cazenave, A., Jevrejeva, S., Alkama, R., Decharme, B., Douville, H., Ablain, M., Beckley, B., 2011. Terrestrial waters and sea level variations on interannual time scale. Glob. Planet. Chang. 75, 76–82. https://doi.org/10.1016/j.gloplacha.2010.10.008.
Luo, X.L., Zeng, E.Y., Ji, R.Y., Wang, C.P., 2007. Effects of in-channel sand excavation on the hydrology of the Pearl River Delta, China. J. Hydrol. 343, 230–239. https://doi.org/10.1016/j.jhydrol.2007.06.019.
Mann, H.B., 1945. Nonparametric tests against trend. Econometrica 13, 245–259.
Mao, Q.W., Shi, P., Yin, K.D., Gan, J.P., Qi, Y.Q., 2004. Tides and tidal currents in the Pearl River estuary. Cont. Shelf Res. 24, 1797–1808. https://doi.org/10.1016/j.csr.2004.06.008.
Miller, L., Douglas, B.C., 2004. Mass and volume contributions to twentieth-century global sea level rise. Nature 428, 406–409. https://doi.org/10.1038/nature02309.
Nicholls, R.J., Cazenave, A., 2010. Sea-level rise and its impact on coastal zones. Science 328, 1517–1520. https://doi.org/10.1126/science.1185782.
Rignot, E., Velicogna, I., van den Broeke, M.R., Monaghan, A., Lenaerts, J.T.M., 2011. Acceleration of the contribution of the Greenland and Antarctic ice sheets to sea level rise. Geophys. Res. Lett. 38, L05503. https://doi.org/10.1029/2011GL046583.
Sassi, M.G., Hoitink, A.J.F., 2013. River flow controls on tides and tide-mean water level profiles in a tidal freshwater river. J. Geophys. Res. 118, 4139–4151. https://doi.org/10.1002/Jgrc.20297.
Sayol, J.M., Marcos, M., 2018. Assessing flood risk under sea level rise and extreme sea levels scenarios: application to the Ebro Delta (Spain). J. Geophys. Res. 123, 794–811. https://doi.org/10.1002/2017JC013355.
Schuttelaars, H.M., de Jonge, V.N., Chernetsky, A., 2013. Improving the predictive power when modelling physical effects of human interventions in estuarine systems. Ocean Coast. Manag. 79, 70–82. https://doi.org/10.1016/j.ocecoaman.2012.05.009.
Susnik, J., Vamvakeridou-Lyroudia, L.S., Baumert, N., Kloos, J., Renaud, F.G., Jeunesse, I., Mabrouk, B., Savic, D.A., Kapelan, Z., Ludwig, R., Fischer, G., Roson, R., Zografos, C., 2015. Interdisciplinary assessment of sea-level rise and climate change impacts on the lower Nile delta, Egypt. Sci. Total Environ. 503, 279–288. https://doi.org/10.1016/j.scitotenv.2014.06.111.
Syvitski, J.P.M., Kettner, A.J., Overeem, I., Hutton, E.W.H., Hannon, M.T., Brakenridge, G.R., Day, J., Vorosmarty, C., Saito, Y., Giosan, L., Nicholls, R.J., 2009. Sinking deltas due to human activities. Nat. Geosci. 2, 681–686. https://doi.org/10.1038/NGEO629.
Tessler, Z.D., Vorosmarty, C.J., Overeem, I., Syvitski, J.P.M., 2018. A model of water and sediment balance as determinants of relative sea level rise in contemporary and future deltas. Geomorphology 305, 209–220. https://doi.org/10.1016/j.geomorph.2017.09.040.
Vellinga, N.E., Hoitink, A.J.F., van der Vegt, M., Zhang, W., Hoekstra, P., 2014. Human impacts on tides overwhelm the effect of sea level rise on extreme water levels in the Rhine-Meuse delta. Coast. Eng. 90, 40–50. https://doi.org/10.1016/j.coastaleng.2014.04.005.
Wang, L., Li, Q., zhong Mao, X., Bi, H., Yin, P., 2018a. Interannual sea level variability in the Pearl River estuary and its response to El NioSouthern oscillation. Glob. Planet. Chang. 162, 163–174. https://doi.org/10.1016/j.gloplacha.2018.01.007.
Wang, Q.S., Pan, C.H., Zhang, G.Z., 2018b. Impact of and adaptation strategies for sea-level rise on Yangtze River Delta. Adv. Clim. Change Res. 9, 154–160. https://doi.org/10.1016/j.accre.2018.05.005.
Wang, Z.B., Van Maren, D.S., Ding, P.X., Yang, S.L., Van Prooijen, B.C., De Vet, P.L.M., Winterwerp, J.C., De Vriend, H.J., Stive, M.J.F., He, Q., 2015. Human impacts on morphodynamic thresholds in estuarine systems. Cont. Shelf Res. 111, 174–183. https://doi.org/10.1016/j.csr.2015.08.009.
Wolinsky, M.A., Edmonds, D.A., Martin, J., Paola, C., 2010. Delta allometry: growth laws for river deltas. Geophys. Res. Lett. 37https://doi.org/10.1029/2010gl044592. Artn L21403.
Wu, Z.Y., Milliman, J.D., Zhao, D.N., Cao, Z.Y., Zhou, J.Q., Zhou, C.Y., 2018. Geomorphologic changes in the lower Pearl River Delta, 1850–2015, largely due to human activity. Geomorphology 314, 42–54. https://doi.org/10.1016/j.geomorph.2018.05.001.
Wu, C.S., Yang, S.L., Huang, S.C., Mu, J.B., 2016a. Delta changes in the Pearl River estuary and its response to human activities (1954-2008). Quat. Int. 392, 147–154. https://doi.org/10.1016/j.quaint.2015.04.009.
Wu, Z.Y., Milliman, J.D., Zhao, D.N., Zhou, J.Q., Yao, C.H., 2014. Recent geomorphic change in LingDing bay, China, in response to economic and urban growth on the Pearl River Delta, southern China. Glob. Planet. Chang. 123, 1–12. https://doi.org/10.1016/j.gloplacha.2014.10.009.
Wu, Z.Y., Saito, Y., Zhao, D.N., Zhou, J.Q., Cao, Z.Y., Li, S.J., Shang, J.H., Liang, Y.Y., 2016b. Impact of human activities on subaqueous topographic change in Lingding Bay of the Pearl River estuary, China, during 1955-2013. Sci. Rep. 6https://doi.org/10.1038/Srep37742. Artn 37742.
Zhang, W., Cao, Y., Zhu, Y., Zheng, J., Ji, X., Xu, Y., Wu, Y., Hoitink, A., 2018. Unravelling the causes of tidal asymmetry in deltas. J. Hydrol. 564, 588–604. https://doi.org/10.1016/j.jhydrol.2018.07.023.
Zhang, W., Cao, Y., Zhu, Y.L., Wu, Y., Ji, X.M., He, Y., Xu, Y.W., Wang, W.G., 2017. Flood frequency analysis for alterations of extreme maximum water levels in the Pearl River Delta. Ocean Eng. 129, 117–132. https://doi.org/10.1016/j.oceaneng.2016.11.013.
Zhang, W., Ruan, X.H., Zheng, J.H., Zhu, Y.L., Wu, H.X., 2010. Long-term change in tidal dynamics and its cause in the Pearl River Delta, China. Geomorphology 120, 209–223. https://doi.org/10.1016/j.geomorph.2010.03.031.
Zhang, W., Wang, W.G., Zheng, J.H., Wang, H.G., Wang, G., Zhang, J.S., 2015a. Reconstruction of stage-discharge relationships and analysis of hydraulic geometry variations: the case study of the Pearl River Delta, China. Glob. Planet. Chang. 125, 60–70. https://doi.org/10.1016/j.gloplacha.2014.12.004.
Zhang, W., Xu, Y., Hoitink, A.J.F., Sassi, M.G., Zheng, J.H., Chen, X.W., Zhang, C., 2015b. Morphological change in the Pearl River Delta, China. Mar. Geol. 363, 202–219. https://doi.org/10.1016/j.margeo.2015.02.012.
Zhang, W., Yan, Y.X., Zheng, J.H., Li, L., Dong, X., Cai, H.J., 2009. Temporal and spatial variability of annual extreme water level in the Pearl River Delta region, China. Glob. Planet. Chang. 69, 35–47. https://doi.org/10.1016/j.gloplacha.2009.07.003.
Zhou, Z., Coco, G., Townend, I., Gong, Z., Wang, Z., Zhang, C., 2018. On the stability relationships between tidal asymmetry and morphologies of tidal basins and estuaries. Earth Surf. Proc. Land. 43, 1943–1959,. https://doi.org/10.1002/esp.4366.
Zhou, Z., Coco, G., Townend, I., Olabarrieta, M., van der Wegen, M., Gong, Z., D'Alpaos, A., Gao, S., Jaffe, B.E., Gelfenbaum, G., He, Q., Wang, Y., Lanzoni, S., Wang, Z.B., Winterwerp, H., Zhang, C., 2017. Is "morphodynamic equilibrium" an oxymoron. Earth-Sci. Rev. 165, 257–267. https://doi.org/10.1016/j.earscirev.2016.12.002.